An Accuracy based Comparison of Three Brain Extraction Algorithms

Gayatri Mirajkar
Yashoda Technical Campus
Wadhe, Satara
gayatri9i@ieee.org

ABSTRACT
Skull stripping is an important image processing step in many neuroimaging studies. In this paper, a comparison of three brain extraction algorithms is done, namely Brain Surface Extractor (BSE), skull stripping algorithm using Geodesic Active Contour (GAC), and skull stripping using active contours without edges. The comparison is done with respect to accuracy of the three algorithms. The results provided by the three algorithms are compared against the processed results available in the OASIS dataset. A comparison of the three algorithms shows that BSE provides the best results with respect to the percentage of non-brain matter contained in the final segmented output. The algorithm using GAC produces a conservative result containing some amount of non-brain matter that can be removed using morphological operator. The algorithm using active contours without edges produces segmentation results containing some amount of brain matter removed from the result. This is mainly due to the sensitivity of the active contour to intensity values in the sulci present in the brain magnetic resonance image.

General Terms
Digital Image Processing, Algorithms

Keywords
Magnetic resonance imaging, skull stripping, active contours, geodesic active contours, level sets

1. INTRODUCTION
Intracranial segmentation commonly referred to as skull stripping, aims to segment the brain tissue (cortex and cerebellum) from the skull and nonbrain intracranial tissues in magnetic resonance (MR) images of the brain. Skull stripping is an important preprocessing step in neuroimaging analyses because brain images must typically be skull stripped before other processing algorithms such as registration, tissue classification, or bias field correction can be applied. In practice, skull stripping is widely used in neuroimaging analyses such as multimodality image fusion and intersubject image comparisons, examination of the progression of brain disorders such as Alzheimer's disease, multiple sclerosis, and schizophrenia, monitoring the development or ageing of the brain, and creating probabilistic atlases from large groups of subjects [1].

A number of factors complicate the problem of segmenting the skull in MRI volumes. These include partial volume effects, variable topology of the skull between individuals, regions of the skull with very high curvature, and regions of the skull whose thickness is small compared to voxel size [11]. Segmentation of brain/non-brain tissue is also one of the most time-consuming preprocessing steps performed in neuroimaging laboratories, and numerous brain extraction algorithms (BEAs) have been developed to perform this step automatically. While BEA's speed up overall image processing, their output varies greatly and can affect the results of subsequent image analysis.

Skull-stripping methods can generally be categorized into three types: intensity based, morphology based and deformable model based. Intensity-based methods rely upon modeling the intensity distribution used for threshold classification. In [2], a semiautomated classification method is proposed for brain tissue classification in brain MR images. This method used intensity distribution functions to identify major brain tissues (e.g., CSF, GM, and WM). Each brain tissue was modeled using a modified log-normal distribution function. The limitation for intensity-based methods is that they are frequently sensitive to intensity bias caused by magnetic field inhomogeneities, sequence variations, scanner drift, or random noise.

Morphology-based methods frequently combine connectivity-based morphological operations and thresholding or edge-detection to extract image features and identify brain surfaces. In [3], a 2D-skull stripping method was proposed which was applied to a midsaggital slice. This method was later extended in [4] to all slices in a saggital series. First, thresholds were used to separate dark pixels (e.g., background, skull and cavities, etc.), then brain regions were identified using a connectivity-based algorithm. Brain Surface Extractor (BSE) [5] is a popular tool which uses a combination of edge-detectors and morphological operators to skull-strip the brain. A potential disadvantage of these methods is that they are often dependent upon many parameters, and the parameters are often empirically generated and sensitive to small changes in the data.

Skull-stripping methods based upon deformable models typically evolve and deform an active contour to fit the brain surface, which is identified using selected image characteristics. In [6], a 2D contour is evolved by maximizing its corresponding 1D optimization problem which was obtained via geometrical transformation from a 2D contour using dynamic programming techniques. The 1D optimization problem was described by a cost function that consisted of six terms including intensity value, morphology, gradient, moving speed of the contour, and smoothness of the contour. In [7], a system of two level set equations, whose zero level curves represented their inner and outer boundaries of the gray matter of the cortex was presented. Each level set equation was driven towards the inner and outer boundaries by a force term determined by the intensity distribution of brain tissues (i.e., CSF, WM and GM). The two level set equations were further related to each other by constraining

the distance between the inner and outer boundaries (i.e., the thickness of gray matter). In [8], an active contour algorithm that uses the level set methods to evolve the active contour was proposed. A fuzzy membership function was used to classify images into four components: WM, GM, CSF and background followed by a gradient detector and a deformable model to evolve an active contour to fit the surface between the CSF and GM. In [9], brain data is registered to an atlas and the brain surface from the atlas is used as the initial contour. Then, an equation based on the level set method was used, in which the speed term was determined by the curvature of the evolving curve and by a sign function that signaled whether to include or exclude a pixel that the curve passed. [10] proposed an automated deformable model for skull stripping, called the brain extraction tool (BET), in which a set of forces were applied in the tangential and normal directions of the evolving surface. In general, deformable models have the potential to produce more robust and accurate skull-stripping results than methods using edge detection and threshold classification. Hybrid schemes have also been proposed to combine multiple results of different algorithms to compensate for problems encountered with individual methods [11].

The main objective of this paper is to compare three brain stripping algorithms with respect to their accuracy of segmentation. The first is based on a level sets representation of geodesic active contours (GAC) [12-14]. The second is based on the minimization of the Mumford-Shah function developed by Chan and Vese [15]. The third BEA is Brain Surface Extractor [5]. Section 2 deals with a description of GAC followed by segmentation using GAC in section 3. Section 4 deals with a description of active contours without edges followed by a brief description of BSE in section 5. The results and discussion are given in section 6.

2. GEODESIC ACTIVE CONTOURS

A novel scheme based on a level sets representation of the GAC model [12-14] is considered for segmentation of brain matter from the MR image of the human brain. This approach is based on the relation between active contours and the computation of geodesics (minimal length curves). The technique is to evolve the contour from inside the MR image under the influence of geometric measures of the MR image. GACs combine the energy minimization approach of the classical "snakes" and the geometric active contours based on curve evolution.

Let $\gamma(t)$ be the curve that has to gravitate towards the boundary of any object at a particular time t. The time t corresponds to the iteration number. Let ψ be a function defined as a signed distance function from the curve $\gamma(t)$. Thus, $\psi(x, y)$ = distance of point (x, y) to the curve $\gamma(t)$.

$$\psi(x,y) = \begin{cases} 0 & ,if\ (x,y) is\ on\ the\ curve \\ < 0 & ,if\ (x,y) is\ inside\ the\ curve \\ > 0 & ,if\ (x,y) is\ outside\ the\ curve \end{cases} \quad (1)$$

ψ is of the same dimension as that of the image $I(x, y)$ that is to be segmented. The curve $\gamma(t)$ is a level-set of the function ψ. Level sets are the set of all points in ψ where ψ = some constant. Thus, $\psi = 0$ is the zeroth level set, $\psi = 1$ is the first level set and so on. ψ is the implicit representation of the curve $\gamma(t)$ and is called as the embedding function since it embeds the evolution of $\gamma(t)$. The embedding function evolves under the influence of image gradients and regions characteristics so that the curve $\gamma(t)$ approaches the boundary of the object. Thus instead of evolving the parametric curve $\gamma(t)$ (e.g., the Lagrangian approach used in snakes), the embedding function itself is evolved. In our algorithm, the initial curve $\gamma(t)$ is a polygon initialized near the boundary of the skull.

Let the curve $\gamma(t)$ be the zeroth-level set of the embedding function. This implies that,

$$\frac{d\psi}{dt} = 0$$

By the chain rule,

$$\frac{d\psi}{dt} = \frac{\partial\psi}{\partial x}\frac{dx}{dt} + \frac{\partial\psi}{\partial y}\frac{dy}{dt} + \frac{\partial\psi}{\partial t}$$

i.e.,

$$\frac{d\psi}{dt} = -\nabla\psi \cdot \gamma'(t)$$

Splitting the $\gamma'(t)$ in the normal $(N(t))$ and tangential $(T(t))$ directions,

$$\frac{\partial\psi}{\partial t} = -\nabla\psi \cdot (v_N N(t) + v_T T(t))$$

Now, since $\nabla\psi$ is perpendicular to the tangent to $\gamma(t)$,

$$\frac{\partial\psi}{\partial t} = -\nabla\psi \cdot (v_N N(t)) \quad (2)$$

The normal component is given by,

$$N = \frac{\nabla\psi}{\|\nabla\psi\|}$$

Substituting this in exp. (2),

$$\frac{\partial\psi}{\partial t} = -\left(div\left(K\frac{\nabla\psi}{\|\nabla\psi\|}\right) + cK\right)\|\nabla\psi\|$$

Thus, the evolution equation for ψ_t such that $\gamma(t)$ remains the zeroth level set is given by,

$$\psi_t = -K(c + \epsilon\kappa)\|\nabla\psi\| + \nabla\psi \cdot \nabla K \quad (3)$$

Where, K, the stopping term for the evolution is an image dependent force and is used to decelerate the evolution near the boundaries, c is the velocity of the evolution, ϵ indicates the degree of smoothness of the level-sets, and κ is the curvature of the level sets computed as,

$$\kappa = -\frac{\psi_{xx}\psi_y^2 - 2\psi_x\psi_y\psi_{xy} + \psi_{yy}\psi_x^2}{(\psi_x^2 + \psi_y^2)^{\frac{3}{2}}}$$

Where ψ_x is the gradient of the image in the *x* direction, ψ_y is the gradient of the image in the *y* direction, ψ_{xx} is the second-order gradient in the *x* direction, ψ_{yy} is the second-order gradient in the *y* direction and ψ_{xy} is the second-order gradient first in the *x* direction, then in *y* direction. Exp. (3) is the level-set representation of the GAC model. This means that the level-set C of ψ is evolving according to,

$$C_t = K(c + \epsilon\kappa)\bar{N} - (\nabla K \cdot \bar{N})\bar{N} \quad (4)$$

Where $\bar{N}$ is the normal to the curve. The first term $(\kappa\bar{N})$ provides the smoothing constraints on the level sets by reducing the total curvature of the level sets. The second term $(c\bar{N})$ acts like a balloon force and it pushes the curve outward towards the object boundary. The goal of the stopping function is to slow down the evolution when it reaches the boundaries. However, the evolution of the curve will terminate only when $K = 0$, i.e., near an ideal edge. In most images, the gradient values will be different along the edge, thus, necessitating different *K* values. In order to circumvent this issue, the third geodesic term $(\nabla K \cdot \bar{N})$ is necessary so

that the curve is attracted towards the boundaries (∇K points towards the middle of the boundary). This term makes it possible to terminate the evolution process even if (a) the stopping function has different values along the edges, and (b) gaps are present in the stopping function.

The stopping term used for the evolution of level sets is given by

$$K(x,y) = \frac{1}{1+\left(\frac{\|\nabla(G(x,y)*I(x,y)\|^{\alpha}}{\kappa}\right)} \quad (5)$$

Where $I(x,y)$ is the image to be segmented, and κ and α are constants. As can be seen, this term $K(x,y)$ is not a function of *t*.

3. SEGMENTATION USING GAC

The brain extraction algorithm starts by reducing the noise artifacts. This is achieved using a Perona-Malik anisotropic diffusion filter [16] applied to the MR image. This has the effect of noise reduction without blurring the edges. By running the diffusion with an edge-seeking diffusion coefficient for a certain number of iterations, the image is evolved towards a piecewise constant image with the boundaries between the constant components being detected as edges.

The stopping function is obtained from exp. (5). The signed distance function is obtained from a mask that is initialized interactively near the skull boundary. The embedding function ψ is initialized as this signed distance function to $\gamma(t=0)$ which is shown in fig. 3. Discretizing exp. (3) leads to the following expression:

$$\frac{\psi_{i,j}^{t+1}-\psi_{i,j}^{t}}{\Delta t} = -cK_{i,j}\|\nabla\psi^{t}\| - K_{i,j}\left(\epsilon\kappa_{i,j}^{t}\|\nabla\psi^{t}\|\right) + \nabla\psi_{i,j}^{t}\cdot\nabla K_{i,j}^{t} \quad (6)$$

Where Δt is the time step. In our implementation, the time step Δt satisfies the Courant-Friedrichs-Lewy (CFL) condition to permit numerical stability. In particular this condition also assures that the zero level set cannot leave the narrow band in a single iteration. The first term $cK_{i,j}\|\nabla\psi^{t}\|$ on the right hand side of the above equation is the velocity term (advection term) and acts as an inflation force. This term could lead to singularities and, hence, is discretized using upwind finite differences. The upwind scheme for approximating $\|\nabla\psi\|$ is given by,

$$\|\nabla\psi\| = \sqrt{A}$$

$$A = \min\left(D_x^{-}(\psi_{i,j},0)^2\right) + \max\left(D_x^{+}(\psi_{i,j},0)^2\right) + \min\left(D_y^{-}(\psi_{i,j},0)^2\right) + \max\left(D_y^{+}(\psi_{i,j},0)^2\right)$$

Where $D_x^{-}\psi$ is the first-order backward difference of ψ in the *x*-direction, $D_x^{+}\psi$ is the first-order forward difference of ψ in the *x*-direction, $D_y^{-}\psi$ is the first-order backward difference of ψ in the *y*-direction and $D_y^{+}\psi$ is the first-order forward difference of ψ in the *y*-direction. The second term $(K_{i,j}\left(\epsilon\kappa_{i,j}^{t}\|\nabla\psi^{t}\|\right))$ is a curvature-based smoothing term and can be discretized using central differences. The third geodesic term $(\nabla\psi_{i,j}^{t}\cdot\nabla K_{i,j}^{t})$ is also discretized using central differences.

After evolving the embedding function ψ according to exp. (6), the curve starts to grow until it satisfies the stopping criterion defined by the stopping function K. Since during the evolution process, the primary interest is in the zeroth level set of ψ, the embedding function can be evolved only in a narrowband around the zeroth level set [14]. This accelerates the evolution process dramatically. During the evolution process, the contour is evolved around a small narrowband around the contour. The evolution process is not uniform across the contour but can vary due to obstacles such as changes in the intensity level.

The level set function was initialized as a signed distance function for computational efficiency. The narrow band extension only evolved the level sets within the band and left other level sets unchanged, which caused the function ψ to no longer represent the distance to the zero level set. So, the level set function ψ was reinitialized periodically to approximate the signed distance from the new contour.

A fast method to rectify ψ as proposed in [17] is given by,

$$\psi_t = S_\varepsilon(\psi')(1-|\nabla\psi|) = S_\varepsilon(\psi_0')\left(1-\sqrt{\psi_x^2+\psi_y^2}\right)$$

$$S_\varepsilon(\psi_0') = \frac{\psi_0'}{\sqrt{\psi_0'^2+\varepsilon^2}}$$

Where ψ_0' is the level set function whose value drifted away from the signed distance. The method proposed in [16] rectified ψ_0' to a distance function while keeping its zero-level curve. Our experiments showed that this method was fast. In that, only one iteration was typically required for ψ to converge to a signed distance function.

4. ACTIVE CONTOURS WITHOUT EDGES

The basic idea in active contour models or snakes is to evolve a curve, subject to constraints from a given image u_0, in order to detect objects in an image. Let Ω be a bounded open subset of $\mathbb{R}^2$ with $\partial\omega$ as its boundary. Let $u_0:\bar{\Omega}\to\mathbb{R}$ be a given image, and $C(s):[0,1]\to\mathbb{R}^2$ be a parametrized curve. Let us also define the evolving curve C in Ω, as the boundary of an open subset ω of Ω (i.e., $\omega\subset\Omega$, and $C=\partial\omega$. In what follows, $inside(C)$ denotes the region ω, and $outside(C)$ denotes the region $\Omega\backslash\bar{\omega}$.

In [15], the method comprises a minimization of an energy-based-segmentation. The idea of the model can be explained in a simple manner. Assume that the image u_0 is formed by two regions of approximately piecewise-constant intensities, of distinct values u_0^i and u_0^o. Assume further that the object to be detected is represented by the region with the value u_0^i. Let denote its boundary by C_0. Then $u_0\approx u_0^i$ inside the object [or $inside(C_0)$] and $u_0\approx u_0^o$ outside the object [or $outside(C_0)$]. Consider the following fitting term:

$$F_1(C)+F_2(C) = \int_{inside\ (C)}|u_0(x,y)-c_1|^2dxdy + \int_{outside\ (C)}|u_0(x,y)-c_2|^2dxdy \quad (7)$$

Where C is any other variable curve, and the constants c_1, c_2, depending on C, are the averages of u_0 inside C and outside C respectively. C_0, the boundary of the object is the minimize of the fitting term,

$$\inf_C\{F_1(C)+F_2(C)\}\approx 0\approx F_1(C_0)+F_2(C_0)$$

In the active contour model of [15], the above fitting term is minimized and regularizing terms are added such as the length of the curve C and (or) the area of the region inside C. The following energy functional $F(c_1, c_2, C)$ is introduced in [15]:

$$F(c_1, c_2, C) = \mu \cdot Length(C) + \upsilon \cdot Area\big(inside(C)\big) + \int_{inside\ (C)} |u_0(x,y) - c_1|^2 dxdy + \int_{outside\ (C)} |u_0(x,y) - c_2|^2 dxdy \quad (8)$$

Where $\mu \geq 0, \upsilon \geq 0, \lambda_1, \lambda_2 > 0$ are fixed parameters. In the numerical calculations of [15], $\lambda_1 = \lambda_2 = 1$ and $\upsilon = 0$. Therefore, the minimization problem considered is

$$\inf_{c_1, c_2, C} F(c_1, c_2, C)$$

The active contour model with $\upsilon \geq 0$ and $\lambda_1 = \lambda_2 = \lambda$ is a particular case of the Mumford-Shah minimal partition problem in which the search is carried out for the best approximation u of u_0, as a function taking only two values, namely

$$u = \begin{cases} average(u_0)\ inside\ C \\ average(u_0)\ outside\ C \end{cases} \quad (9)$$

And with one edge C, represented by the snake or the active contour. This particular case of the minimal partition problem is formulated and solved using the level set method [15].

In the level set method [18], $C \subset \Omega$ is represented by the zero-level set of a Lipschitz function $\phi: \Omega \to \mathbb{R}$, such that

$$\begin{cases} C = \partial\omega = \{(x,y) \in \Omega : \phi(x,y) = 0\} \\ inside(C) = \omega = \{(x,y) \in \Omega : \phi(x,y) > 0\} \\ outside(C) = \Omega \backslash \bar{\omega} = \{(x,y) \in \Omega : \phi(x,y) < 0\} \end{cases}$$

Where $\omega \subset \Omega$ is open and $C = \partial\omega$. For the level set formulation of the variational active contour model, the unknown variable C is replaced by the unknown variable ϕ. Using the Heaviside function, H, and the one-dimensional Dirac measure δ_0, and defined, respectively, by

$$H(z) = \begin{cases} 1, & if\ z \geq 0 \\ 0, & if\ z < 0 \end{cases}$$

$$\delta_0 = \frac{d}{dz} H(z)$$

the energy function F is expressed in the following manner.

$$F(c_1, c_2, \phi) = \mu \int_\Omega \delta(\phi(x,y)) |\nabla\phi(x,y)| dxdy + \upsilon \int_\Omega H\big(\phi(x,y)\big) dxdy + \lambda_1 \int_\Omega |u_0(x,y) - c_1|^2 H\big(\phi(x,y)\big) dxdy + \lambda_2 \int_\Omega |u_0(x,y) - c_2|^2 \Big(1 - H\big(\phi(x,y)\big)\Big) dxdy \quad (10)$$

As defined in exp. (9), u the solution of our model as a particular case of the Mumford-Shah minimal partition problem can simply be written using the level set formulation as

$$u(x,y) = c_1 H\big(\phi(x,y)\big) + c_2 \Big(1 - H\big(\phi(x,y)\big)\Big), (x,y) \in \bar{\Omega} \quad (11)$$

Keeping ϕ constant and minimizing the energy $F(c_1, c_2, \phi)$ with respect to the constants c_1 and c_2, it is easy to express these constants function of ϕ by

$$c_1(\phi) = \frac{\int_\Omega u_0(x,y) H\big(\phi(x,y)\big) dxdy}{\int_\Omega H\big(\phi(x,y)\big) dxdy} \quad (12)$$

if $\int_\Omega H\big(\phi(x,y)\big) dxdy > 0$ (i.e., if the curve has a nonempty interior in Ω, and

$$c_2(\phi) = \frac{\int_\Omega u_0(x,y)\big(1 - H\big(\phi(x,y)\big)\big) dxdy}{\int_\Omega (1 - H(\phi(x,y))) dxdy} \quad (13)$$

if $\int_\Omega (1 - H(\phi(x,y))) dxdy > 0$ (i.e., if the curve has a nonempty interior in Ω). For the corresponding "degenerate" cases, there are no constraints on the values of c_1 and c_2. Then, c_1 and c_2 are in fact given by

$$\begin{cases} c_1(\phi) = average(u_0)\ in\ \{\phi \geq 0\} \\ c_2(\phi) = average(u_0)\ in\ \{\phi < 0\} \end{cases} \quad (14)$$

The associated Euler-Lagrange expression for ϕ is given below. Parametrizing the descent direction by an artificial time $t \geq 0$, the initial expression in $\phi(t,x,y)$ (with $\phi(0,x,y) = \phi_0(x,y)$ defining the initial contour) is

$$\frac{\partial\phi}{\partial t} = \delta_\epsilon(\phi) \Big[\mu\, \mathrm{div}\Big(\frac{\nabla\phi}{|\nabla\phi|}\Big) - \upsilon - \lambda_1 (u_0 - c_1)^2 + \lambda_2 (u_0 - c_2)^2\Big] = 0\ in\ (0,\infty) \times \Omega,$$
$$\phi(0,x,y) = \phi_0(x,y)\ in\ \Omega$$
$$\frac{\delta_\epsilon(\phi)}{|\nabla\phi|} \frac{\partial\phi}{\partial\bar{n}} = 0\ on\ \partial\Omega \quad (15)$$

The initial contour is initialized interactively near the brain boundary. This initial contour is used to generate the mask from which a signed distance function, i.e., the initial embedding function is created. The embedding function is evolved according to exp. (15). Since, during the evolution process, the primary interest is in the zeroth level set of ϕ, the embedding function can be evolved only in a narrowband around the zeroth level set [14]. Similar to the case of GACs, this accelerates the evolution process. The evolution process is stopped when a stable and stationary solution is obtained. During the evolution process, ϕ is again reinitialized to the signed distance function using the method given in [17].

5. BRAIN SURFACE EXTRACTOR

Brian Surface Extractor (BSE) [5] uses a combination of edge-detectors and morphological operators to skull-strip the brain. BSE employs anisotropic diffusion filtering. A 2D Marr-Hildreth operator employing low-pass filtering with a Gaussian kernel and localization of zero-crossings in the Laplacian of the filtered image was first used to identify anatomic boundaries. Then, morphological operators were used to separate the tissues into component regions. Next, the largest central connected component was extracted as the brain region. Finally, nonbrain structures still attached to the brain region were removed.

Three parameters are user-adjustable: anisotropic smoothing kernel (ASK: default = 25), number of iterations (ITER, default = 3), and edge detection σ (default = 0.64).

6. RESULTS AND DISCUSSION

The brain extraction algorithms using geodesic active contours and Chan-Vese active contours have been developed using MATLAB 2009b on an Intel Pentium Core2Duo machine. The images used for the analysis have been taken from the Open Access Series of Imaging Studies (OASIS) and The Whole Brain Atlas. Out of the two datasets available on the OASIS webpage, the dataset of Cross-sectional MRI Data in Young, Middle Aged, Nondemented and Demented Older Adults is used. Both T1 and T2-weighted MR images are used for the analysis.

The segmentation results for the images from the OASIS dataset are shown in fig. (1). Fig. 1(a) and fig. 1(f) are showing the original images. The slice orientation chosen for analysis is the transaxial or axial orientation. The processed results available in the dataset are shown in fig. 1(b) and fig. 1(g) for the respective images. The Brain Surface Extractor (BSE) algorithm available in the stand alone application BrainSuite was applied to the dataset images. BrainSuite is available for download via http://users.loni.ucla.edu/. The resulting skull stripped images are shown in fig. 1(c) and fig. 1(h). From fig. 1(c) it can be seen that some part of the brain region has been removed by the BSE algorithm. This is not the case with the result obtained by the GAC algorithm in fig. 1(d). Comparing the original image and the result of the GAC algorithm, it can be seen that almost perfect segmentation of the brain has been achieved. On the other hand, the result obtained using Chan-Vese active contours in fig. 1(e) does not fare so well. The result using the GAC algorithm in fig. 1(i) contains some non-brain matter on the left and right sides. This can be easily removed using simple morphological operators.

We observed that GACs perform well as compared to Chan-Vese active contours for skull-stripping. This may be because of the robustness of the stopping function involved in the evolution of the GAC. A well-defined stopping function is able to produce effective segmentation. The accuracy of the GAC can be further observed from fig. 2 which is showing an axial T1-weighted image (fig. 2(a)), axial T2*-weighted image (fig. 2(c)), and axial T2-weighted image (fig. 2(e)). The corresponding skull-stripped images are shown beside these images in fig. 2(b), fig. 2(d), and fig. 2(f) respectively.

The algorithm implementing GACs for segmenting the brain first employs Perona-Malik anisotropic diffusion for pre-processing. This results in a reduction of image noise without removing significant parts of the image content, typically edges, lines and other details that are important for the interpretation of the image. Anisotropic diffusion resembles the process that creates a scale-space, where an image generates a parameterized family of successively more and more blurred images based on the diffusion process. The next step involves the generation of a stopping function from exp. (5). Using morphological operations, a pre-segmentation of the MR image is roughly done into two regions, brain and the background. The centroid of the brain region is obtained. Taking the centroid, an ellipse is drawn which is well inside the region comprising the brain. This ellipse is taken as the initial contour. The signed distance function (SDF) is generated from this contour.

It is observed that the proposed algorithm is able to effectively segment the brain region from both T1-weighted as well as T2-weighted images. The accuracy of the segmentation technique depends on the stopping function generated using exp. (5). The more accurate the stopping function is able to highlight the boundary between the brain and non-brain region, the more accurate the GAC is able to follow the curves in the brain region. The proposed algorithm can segment the brain region from normal brain MR images as well as those containing tumors. The stopping function can be adjusted by varying the parameters κ and α so as to avoid weak boundaries. The presence of a weak boundary or a kink in the detected boundary can cause leakage of the contour through that portion, resulting in incorrect segmentation. In our experiments, we observed that keeping α equal to 8 resulted in a strong boundary between the brain and skull. The value of κ can be varied from 2 to 5 to obtain an optimal reduction of the grayscale information of the brain. Since the initial contour is situated near to the brain-skull interface, the model converges faster and in a fewer number of iterations, thus reducing processing time.

It can be observed that the GAC model is able to effectively overcome the problem of topological changes in the form of tumor regions in the brain image. This can be markedly observed in fig. 2(d) which shows the tumor region as a prominent part. Before obtaining the stopping function for T2-weighted MR images, morphological operations such as erosion and dilation can help to increase the accuracy of the stopping function. This is necessary since for T2-weighted MR images, to obtain a clear demarcation between brain and the surrounding non-brain tissue is difficult because of the intensity values of the corresponding regions. Sometimes, it is difficult to obtain a clear brain-skull boundary due to the gradient involved in the stopping function expression. In this case, increasing the width of the Gaussian filter in exp. (5) solves this problem, but with the added disadvantage of obtaining thick boundaries. This results in a loss of brain tissue in the final segmentation. Therefore the crux of the proposed algorithm is to achieve correct skull stripping results with minimum loss of data.

We have observed that, as compared to other active contour models, segmentation using GAC is more reliable and also depends on less number of parameters. The calculation time is reduced by using narrow-band propagation of the model. The proposed algorithm also displays scope for improvement of the results and for increasing the robustness of the algorithm. The proposed algorithm is also insensitive to random noise scattered in the MR image because the curvature term limits artificially sharp changes in the evolving curve that might be caused by random noise. Additional research is needed to address the potential advantages and limitations of the proposed method.

For the implementation of Chan-Vese active contours, no pre-processing was employed such as morphological filtering. The initial contour was interactively selected to be as much near the brain-skull boundary as possible. This was achieved using the roipoly function available in MATLAB. Here also the user initialized the initial contour near the brain-skull interface thus reducing the number of iterations and also effectively bypassing the structures present within the brain. This also allowed the model to converge in less number of steps For the implementation the parameters chosen are: $\lambda_1 = \lambda_2 = 1, \nu = 0, \mu = 0.2$ and the time step dt is calculated according to the Courant-Fredrichs-Lewy condition. The model converged to a solution after completing the specified number of iterations.

Table 1 presents the performance indices for the three algorithms. Out of the three BSE performs the best with the least FP_rate. The FP_rate is calculated as the number of voxels incorrectly classified as brain tissue by the automated algorithm divided by manually segmented brain masks. Lower

the FP_rate coefficient, the more accurate the segmentation results. The processed results available in the OASIS dataset are taken in this analysis as the gold standard. The results obtained using BSE, GAC algorithm, and Chan-Vese active contour algorithms are compared against this gold standard. It is observed that the FP_rate for the GAC algorithm is slightly larger than the FP_rate for BSE. This is attributed mainly to the conservative nature of the algorithm, i.e., the tendency to avoid removing brain tissue than to remove all non-brain tissues for clinical applications. The performance of the skull-stripping algorithm using Chan-Vese active contours is somewhat poor as compared to both BSE and GACs. This is because of the tendency of the active contour to align itself along the deep sulci of the brain. More work is needed to prevent the model from being sensitive to such intensity changes.

Table 1. Performance index of GAC, Chan-Vese, active contour algorithm and BSE method of skull stripping

Sr. No.	Method	FP_rate
1	GAC	0.0489
2	Chan-Vese Active Contours	0.1369
3	BSE	0.0265

7. CONCLUSION

In this paper, three methods have been compared which are dealing with the problem of skull stripping in MR images of the human brain. Out of the three methods, BSE performs the best with the lowest FP_rate. The algorithm using GAC has a performance comparable to that of BSE but, the results obtained using GAC contained some non-brain matter as well. Hence, post-processing using morphological operators is needed to obtain the final segmented mask. The algorithm using Chan-Vese active contours is too sensitive to the intensity changes and work is being done to improve it.

8. REFERENCES

[1] H. H. Zhuang, D. J. Valentino, and A. W. Toga, "Skull-stripping magnetic resonance images using a model-based level set," NeuroImage, vol. 32, pp. 79 – 82, 2006.

[2] C. DeCarli, J. Maisog, D. G. M. Murphy, D. Teichberg, S. I. Rapoport, and B. Horwitz, "Method for quantification of brain ventricular and subarachnoid CSF volumes from MR images," J. Comput. Assist. Tomogr., vol. 16, no. 2, pp. 274 – 284, 1992

[3] C. Lee, S. Huh, T. A. Keller, and M. Unser, "Unsupervised connectivity-based thresholding segmentation of midsaggital brain MR images," Comput. Biol. Med., vol. 28, pp. 309 – 338, 1998

[4] S. Huh, T. A. Keller, K. H. Sohn, and C. Lee, "Automated cerebrum segmentation from 3-D saggital brain MR images," Comput. Biol. Med., vol. 32, pp. 311 – 328, 2002

[5] D. W. Shuttuck, S. R. Sandor-Leahy, K. A. Schaper, D. A. Rottenburg, and R. M. Leahy, "Magnetic resonance image tissue classification using a partial volume model," NeuroImage, vol. 13, pp. 856 – 876, 2001

[6] G. B. Aboutanos, J. Nikanne, N. Watkins, and B. M. Dawant, "Model creation and deformation for the automatic segmentation of the brain in MR images," IEEE Trans. Biomed. Engg., vol. 46, no. 11, pp. 1346 – 1356, 1999

[7] X. Zeng, L. H. Staib, R. T. Schultz, and J. S. Duncan, "Segmentation and measurement of the cortex from 3-D MR images using coupled-surfaces propagation," IEEE Trans. Med. Imag., vol. 18, no. 10, pp. 927 – 937, 1999

[8] J. S. Suri, "Two-dimensional fast magnetic resonance brain segmentation," IEEE Trans. Med. Biol., pp. 84 – 95, 2001

[9] C. Baillard, P. Hellier, and C. Barillot, "Segmentation of brain 3D MR images using level sets and dense registration," Med. Image Anal., vol. 5, pp. 185 – 194, 2001

[10] S. M. Smith, "Fast robust automated brain extraction," Hum. Brain Mapp., vol. 17, pp. 143 – 155, 2002

[11] H. Rifai, I. Bloch, S. Hutchinson, J. Wiart, and L. Garnero, "Segmentation of the skull in MRI volumes using deformable model and taking the partial volume effect into account," Med. Image Anal., vol. 4, pp. 219 – 233, 2000

[12] S. Shah and A. Ross, "Iris segmentation using geodesic active contours," IEEE Trans. Inf. Foren. & Sec., vol. 4, no. 4, pp. 824 – 836, 2009

[13] J. A. Sethian, "A review of recent numerical algorithms for hypersurfaces moving with curvature dependent speed," J. Different. Geometry, vol. 31, pp. 131 – 161, 1989

[14] R. Malladi, J. A. Sethian, and B. C. Vemuri, "Shape modeling with front propagation: a level set approach," IEEE Trans. Pattern Anal., Mach. Intell., vol. 17, no. 2, pp. 125 – 133, 1995

[15] T. F. Chan and L. A. Vese, "Active contours without edges," IEEE Trans. Image Process., vol. 10, no. 2, pp. 266 – 277, 2001

[16] P. Perona and J. Malik, "Scale-space and edge detection using anisotropic diffusion," IEEE Trans. Pattern Anal. Mach. Intell., vol. 12, no. 7, pp. 629 – 639, 1990

[17] M. Sussman, P. Smereka, and S. Osher, "A level set approach for computing solutions to incompressible two-phase flow," J. Comput. Phys., vol. 114, pp. 146 – 159, 1994

[18] S. Osher and J. A. Sethian, "Fronts propagating with curvature-dependent speed: Algorithms based on Hamilton-Jacobi Formulation," J. Comput. Phys., vol. 79, pp. 12 – 49, 1988

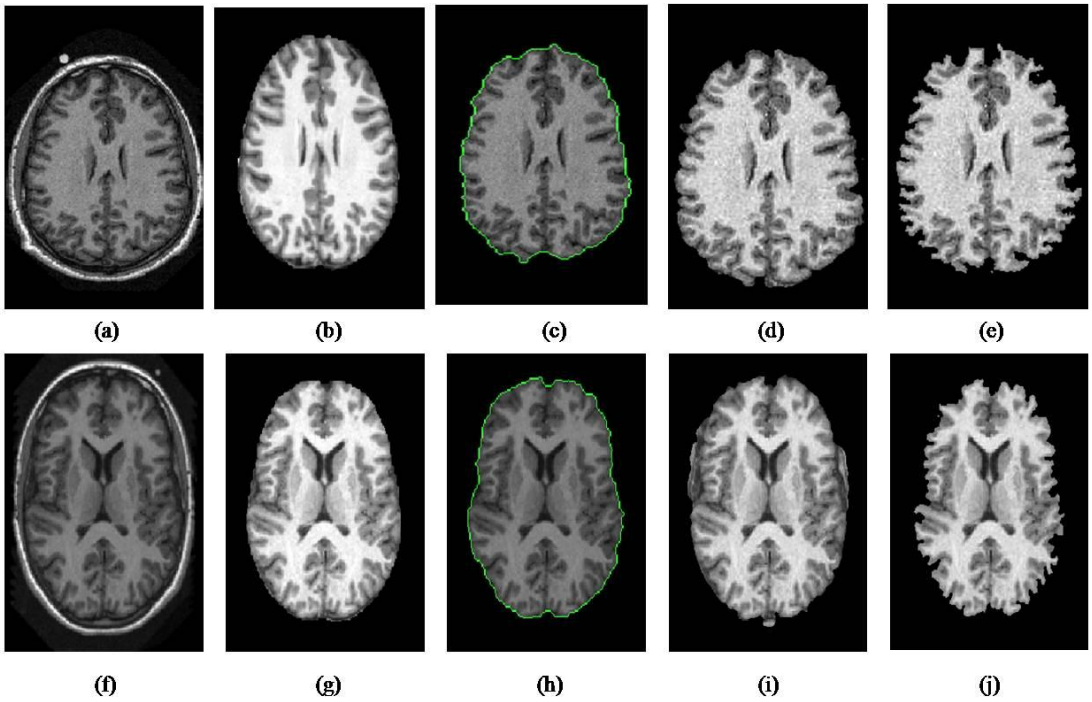

Figure 1. Skull stripping results for the OASIS dataset using BSE, GAC and Chan-Vese active contour

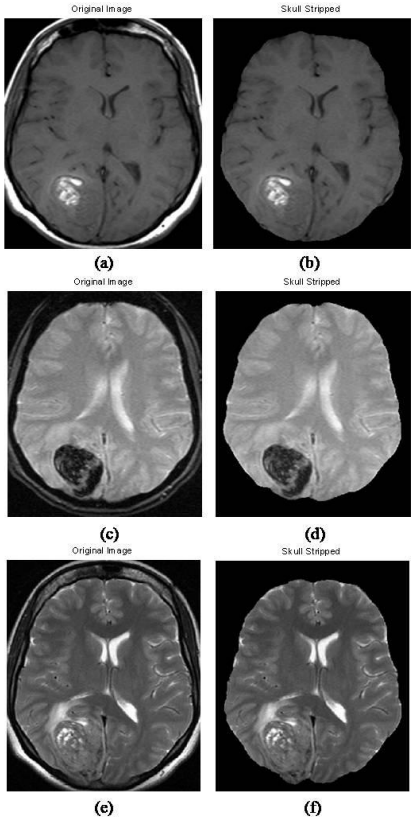

Figure 2. Skull stripping results using GAC for (a), (b) axial T1 weighted, (c), (d) axial T2* weighted, (e), (f) axial T2 Weighted

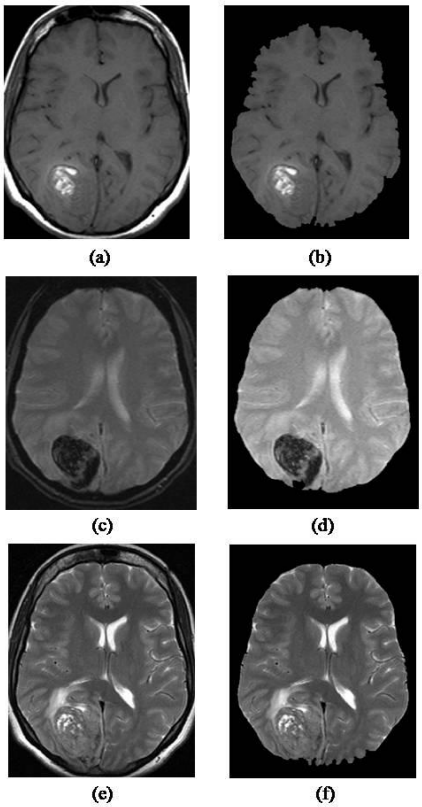

Figure 3. Skull stripping results using Chan-Vese active Contours for (a), (b) axial T1 weighted, (c), (d) axial T2* Weighted, (e), (f) axial T2 weighted